

HyenaPixel: Global Image Context with Convolutions

Julian Spravil¹, Sebastian Houben^{2,1} and Sven Behnke^{3,4,1}

¹Fraunhofer IAIS, Birlinghoven, Germany

²University of Applied Sciences Bonn-Rhein-Sieg, Sankt Augustin, Germany

³University of Bonn, Autonomous Intelligent Systems, Computer Science Institute VI – Intelligent Systems and Robotics – and Center for Robotics, Bonn, Germany

⁴Lamarr Institute for Machine Learning and Artificial Intelligence, Germany

julian.spravil@iais.fraunhofer.de, sebastian.houben@h-brs.de, behnke@cs.uni-bonn.de

Abstract

In vision tasks, a larger effective receptive field (ERF) is associated with better performance. While attention natively supports global context, convolution requires multiple stacked layers and a hierarchical structure for large context. In this work, we extend Hyena, a convolution-based attention replacement, from causal sequences to the non-causal two-dimensional image space. We scale the Hyena convolution kernels beyond the feature map size up to 191×191 to maximize the ERF while maintaining sub-quadratic complexity in the number of pixels. We integrate our two-dimensional Hyena, HyenaPixel, and bidirectional Hyena into the MetaFormer framework. For image categorization, HyenaPixel and bidirectional Hyena achieve a competitive ImageNet-1k top-1 accuracy of 83.0% and 83.5%, respectively, while outperforming other large-kernel networks. Combining HyenaPixel with attention further increases accuracy to 83.6%. We attribute the success of attention to the lack of spatial bias in later stages and support this finding with bidirectional Hyena.

1 Introduction

The 35-year history of Convolutional Neural Networks’ (ConvNets) [LeCun *et al.*, 1989] successful track record [LeCun *et al.*, 1998; Behnke, 2003; Ciresan *et al.*, 2012; Krizhevsky *et al.*, 2012; Szegedy *et al.*, 2015; He *et al.*, 2016; Tan and Le, 2019] recently has been challenged by Vision Transformers (ViTs) [Dosovitskiy *et al.*, 2021]. Many common beliefs about ConvNets are currently being questioned and reassessed under the pressure of competition. There is evidence that disproves the claim that only Transformers with attention [Vaswani *et al.*, 2017] can scale to large data corpora. ConvNets show very similar scaling laws to Transformers in terms of data and model scale [Smith *et al.*, 2023; Liu *et al.*, 2022; Woo *et al.*, 2023]. Furthermore, attention can be replaced with computationally cheaper token mixers while achieving comparable performance. These replacements focus, among others, on the Fourier transform [Lee-Thorp *et al.*, 2022], simple pooling [Yu *et al.*, 2022], or long convolutions with gating, as in Hyena [Poli *et al.*, 2023]. Despite its

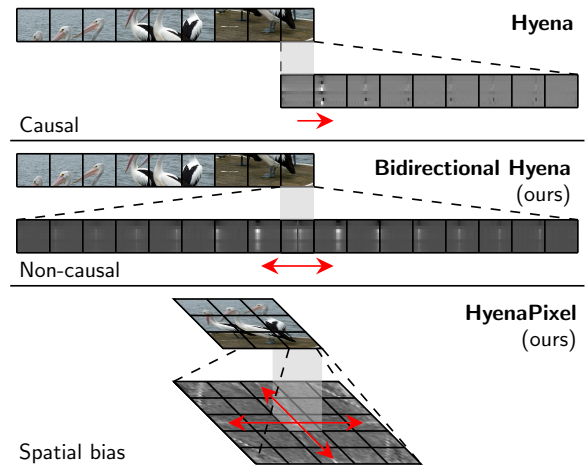


Figure 1: Our extensions of Hyena [Poli *et al.*, 2023] (top). In bidirectional Hyena (center), a large non-causal filter is applied to both sides of the token sequence. HyenaPixel (bottom) uses a large convolutional kernel to process 2D feature maps. We show the evaluation of the rightmost token position and the resulting kernel overlap.

potential, the latter remains largely unexplored. While large kernels were used for better interpretability, they were discarded in favor of stacked small kernels [Szegedy *et al.*, 2015; He *et al.*, 2016; Tan and Le, 2019]. Only recently, large filters were rediscovered for sequence modeling [Poli *et al.*, 2023; Fu *et al.*, 2023] but also for vision with medium [Peng *et al.*, 2017; Liu *et al.*, 2022; Guo *et al.*, 2022] to large kernels sizes—up to 61×61 [Ding *et al.*, 2022; Liu *et al.*, 2023].

Intuitively, attention provides global context by calculating a weighted sum for each token based on its similarity to other tokens [Vaswani *et al.*, 2017]. A convolution filter can be interpreted as learned discrete attention matrices, in which for small kernel sizes most values are zero. In this setting, we ask two research questions: i) Is an approximation of attention with fixed learned attention patterns, like the Hyena operator, a sufficient replacement for fine-granular, fully data-driven attention in vision applications? ii) Does the addition of spatial bias impact performance?

Figure 1 illustrates our approach. We extend the causal convolution-based attention replacement Hyena [Poli *et al.*, 2023] by considering bidirectional, non-causal information

flow—bidirectional Hyena (H_b)—and by accommodating the 2D nature of images with spatial bias—HyenaPixel (H_{px}).

The main contributions of our work are:

- We extend causal convolution-based Hyena [Poli *et al.*, 2023] to non-causal and 2D inputs, while maintaining training stability, sub-quadratic complexity, and enabling large effective receptive fields (ERFs).
- We evaluate the resulting token mixers H_b and H_{px} in the MetaFormer framework for image classification, object detection, and semantic segmentation and achieve results outperforming other large-kernel networks.
- We analyze the learned features of H_{px} , elaborate on the importance of global context, bidirectional modeling and spatial bias with convolution and compare our approach with different token mixer configurations.

2 Related Work

The Vision Transformer (ViTs) [Dosovitskiy *et al.*, 2021] plays a significant role in the recent developments in vision [Tu *et al.*, 2022; Woo *et al.*, 2023; Darcet *et al.*, 2023]. ViTs split an input image into equal-sized patches of size 16×16 and project them into a token space. Positional encoding is added to preserve spatial information. The tokens are processed using the Transformer encoder with bidirectional attention originally proposed by Vaswani *et al.* [2017]. Improvements to ViTs focus on the architecture [Liu *et al.*, 2021; Yu *et al.*, 2022], training strategy [Touvron *et al.*, 2021a; Woo *et al.*, 2023], and on the attention-mechanism or generally token mixing [Liu *et al.*, 2021; Dong *et al.*, 2022; Tu *et al.*, 2022; Yu *et al.*, 2022; Yu *et al.*, 2024]. Hierarchical structure is a commonly applied architecture modification [Liu *et al.*, 2021; Yu *et al.*, 2022; Tu *et al.*, 2022]. Knowledge distillation with an extra teacher token from a CNN teacher also proved helpful [Touvron *et al.*, 2021a]. Swin Transformers [Liu *et al.*, 2021] apply attention to shifted rectangular windows. MaxViT [Tu *et al.*, 2022] uses sparse window attention and grid attention for global interactions. Focus of current research is the self-supervised learning of visual features [Woo *et al.*, 2023].

Substitutes for attention. While attention is a powerful and flexible mechanism, its complexity is quadratic in the number of tokens [Vaswani *et al.*, 2017]. Linear attention [Katharopoulos *et al.*, 2020] uses a kernel formulation to express similarity between tokens. However, finding expressive kernel functions is challenging [Han *et al.*, 2023]. MLP-Mixer [Tolstikhin *et al.*, 2021] uses multiple linear layer stacks applied alternating on the channel and token dimensions. The idea of basic token mixing is further extended to a mean-pooling approach [Yu *et al.*, 2022] and simple convolutional layers [Yu *et al.*, 2024]. FNet [Lee-Thorp *et al.*, 2022] replaces the attention layer with the Fourier transform along the token and channel dimensions. Hyena uses long and short convolutions for causal token mixing [Poli *et al.*, 2023]. They share the same goal as Fu *et al.* [2023] to apply convolutions for efficient training with long token sequences. Convolution appears to be a promising solution for vision-related [Yu *et al.*, 2024] but also sequence-modeling [Poli *et*

al., 2023] tasks as many other alternatives struggle to achieve high performance.

ConvNets and large kernels. The success of Transformers led to new advancements in ConvNet research. Typically, the Transformer architecture is kept while the attention layer is replaced with a combination of convolutional layers [Yu *et al.*, 2022; Yu *et al.*, 2024]. Common across large-kernel networks is their regularization through parameterizing the convolution weights to guarantee smoothness [Romero *et al.*, 2022a; Romero *et al.*, 2022b; Fu *et al.*, 2023; Poli *et al.*, 2023] or by applying sparsity of some form [Dai *et al.*, 2017; Peng *et al.*, 2017; Guo *et al.*, 2022; Liu *et al.*, 2023]. Romero *et al.* [2022a] proposed parameterized filters with dynamic size and discovered that the filter size increases with depth. However, parameterized kernels as used in [Romero *et al.*, 2022a; Romero *et al.*, 2022b; Fu *et al.*, 2023; Poli *et al.*, 2023] require assumptions about how the input is processed, potentially hurting performance. The global convolution network [Peng *et al.*, 2017] applies separable convolutions (21×1 and 1×21) to improve classification while maintaining localization for semantic segmentation. SegNeXt [Guo *et al.*, 2022] also utilizes parallel separable convolutions with sizes between 7 and 21. RepLKNet [Ding *et al.*, 2022] uses full convolutions with size up to 31×31 , while the large kernels are fused by reparameterization of multiple smaller kernels. SLaK [Liu *et al.*, 2023] uses two parallel kernels spanning 61×5 with dynamic sparsity. Lui *et al.* use sparsity to train significantly wider networks, theoretically allowing the training and inference of larger models while keeping the Floating Point Operations (FLOP) low, however, in reality, an efficient hardware implementation is still being sought.

The simultaneous work by Zimerman and Wolf [2023], like ours, aims to raise the dimensional extent of Hyena to higher dimensions and maintains the implicit long convolution filters. The authors use an implicit filter formulation based on 2D positional embeddings. Evaluation is conducted on small-scale datasets in different Transformer frameworks. Their approach improved the performance over their baselines but also benefited from additional subsequent attention layers. The causality of Hyena is addressed by rotating the input after each layer. We propose a non-causal Hyena layer that does not require input transformations like rotation and can be also applied to higher-dimensional input. While the authors show improved performance for small datasets by adding spatial bias, we find the opposite for larger data corpora. In this case, we show that sequential bidirectional data modeling is superior.

3 Method

Motivation. Vision Transformers (ViTs) are one point ahead of Convolutional Neural Networks (ConvNets): A single attention layer already has global context. Current ConvNets scale kernels to at most 61×61 [Ding *et al.*, 2022; Liu *et al.*, 2023] and thus only give the center pixel full context. Kernels that are larger than the feature map, however, proved beneficial [Ding *et al.*, 2022]. A recent approach designed for language modeling promises global context based

on gated global convolution, namely the Hyena operator [Poli *et al.*, 2023]. Motivated by Hyena’s promising properties for sequence modeling, we apply it to the 2D pixel space with drastically larger kernels than previously considered.

Hyena. The Hyena operator by Poli *et al.* [2023] first projects the input sequence x of length L into different spaces $p_0(x), \dots, p_O(x)$. The number of projections is determined by the order parameter O . The projection $p_i(\cdot)$ is defined by a linear layer and a local convolution. Aggregation of the output is handled recursively by element-wise multiplication of the previous result with the next projection:

$$y_{i+1} = g(y_i) \cdot p_{i+2}(x). \quad (1)$$

Intermediate results are convolved with a large implicit filter, handled by function $g(\cdot)$. The initial value is set to $y_0 = p_0(x) \cdot p_1(x)$. The kernel weights of the global convolution are implicitly modeled by applying a Feed-Forward Network (FFN) with a sinusoidal activation function to a positional embedding. The positional embedding is a truncated complex exponential basis $\rho_k(t) = e^{i2\pi kt/L}$ for $k = 0, \dots, K - 1$, where K represents the embedding dimension. Furthermore, the resulting filter is regularized by modulation with an exponential decay

$$\text{Window}(t) = \exp\{-\alpha t\} + b, \quad (2)$$

with scaling factor α , bias b and $t = 0, 1, \dots, L - 1$. Causality is achieved by circularizing the filter by zero-padding to length $2L - 1$ and keeping the L left output positions of the circular FFT-based convolution. In this work, we simplify the Hyena operator by setting $O = 2$. With this simplification, we can rewrite the recursive formulation as follows:

$$y = g(q \cdot k) \cdot v, \quad (3)$$

with query $q = p_0(x)$, key $k = p_1(x)$ and value $v = p_2(x)$.

Bi-directional Hyena (H_b). The concept of causality, i.e. the next token in a sequence can only refer to the previous tokens, is very useful for autoregressive language modeling but unnatural for offline-processing of signals. Therefore, we extend the Hyena operator to bidirectional sequence modeling. This requires larger filters and an evaluation region centered around current sequence element. In detail, the filter width is increased from sequence length L to $2L - 1$ to have full sequence coverage at each token position. Hyena pads the filter and input with zeros to $2L - 1$, which, in our case, is only required for the input. Instead of selecting the output indices $0, 1, \dots, L - 1$ of the circular FFT-based convolution, we select the indices $\frac{L}{2}, \frac{L}{2} + 1, \dots, L + \frac{L}{2}$ to obtain a centered filter. The modulation of the filter $\text{Window}(t)$ can be set to $\exp\{-\alpha|t|\} + b$ with $t = -L + 1, -L + 2, \dots, 0, \dots, L - 1$. Note that the complexity is the same as for the causal Hyena operator, i.e. $\mathcal{O}(L \log_2 L)$. We name the resulting operator H_b .

HyenaPixel (H_{px}). Images are two-dimensional and could therefore benefit from spatial bias. To add spatial bias to H_b , we replace $\text{Window}(t)$ (cf. Equation 2) with

$$\text{Window}(t_x, t_y) = \exp\left\{-\alpha\sqrt{(t_x - c_x)^2 + (t_y - c_y)^2}\right\} + b. \quad (4)$$

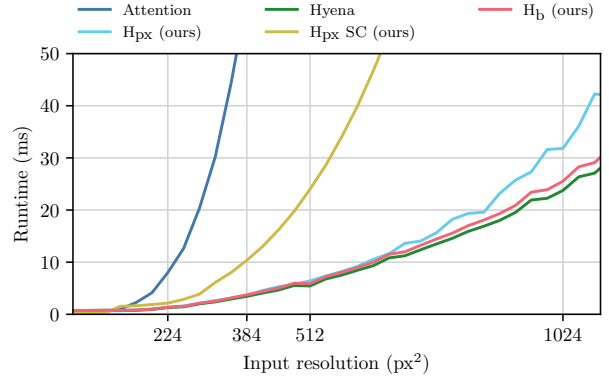


Figure 2: Runtime scaling of components with global token interactions. Input images are patched with a patch size of 4. H_{px} SC uses separable convolutions (SC) instead of an implicit filter. The experiment was conducted on an Nvidia A100 GPU.

where c_x and c_y is the filter center. We use the 2D extension of the 1D positional encoding of the original Transformer proposed by Wang *et al.* [2021]. Positions are encoded in the vertical and horizontal direction using sine and cosine functions. The inputs to the circular 2D FFT convolution are zero padded to $(2L_x - 1) \times (2L_y - 1)$. The asymptotic complexity of H_{px} is $\mathcal{O}(L_x L_y \log_2(L_x L_y))$. In practice, however, H_{px} is slightly slower while the performance only differs marginally for resolutions below 512 px^2 , cf. Figure 2. We name this extension HyenaPixel (H_{px}).

Hierarchical Transformer. We embed H_b and H_{px} in a Transformer encoder [Vaswani *et al.*, 2017; Dosovitskiy *et al.*, 2021], considering four frameworks: the original isomorphic ViT [Dosovitskiy *et al.*, 2021] and three hierarchical models MetaFormer [Yu *et al.*, 2022; Yu *et al.*, 2024], ConvNeXt [Liu *et al.*, 2022; Woo *et al.*, 2023], and Swin Transformer [Liu *et al.*, 2021]. However, because hierarchical models consistently perform better than their isomorphic counterparts [Liu *et al.*, 2022] and MetaFormer already explored different token mixer types, we settled on the MetaFormer architecture, as depicted in Figure 3.

There are a few key differences to the Swin Transformer: First, the image patching layer and the in-between patch merging layers have an overlap (i.e. the kernel size is larger than the stride). Second, the depth of the network is increased while the width is decreased. Finally, the commonly used activation function GELU [Hendrycks and Gimpel, 2016] is replaced with StarReLU [Yu *et al.*, 2024].

Model sizes. We explore the following model sizes:

- S4: $C = (64, 128, 320, 512)$, $B = (1, 1, 1, 1)$;
- S12: $C = (64, 128, 320, 512)$, $B = (2, 2, 6, 2)$; and
- S18: $C = (64, 128, 320, 512)$, $B = (3, 3, 9, 3)$.

Here, C is the channel dimension and B is the number of blocks per stage. We use the syntax of Yu *et al.* [2024] and classify the channel dimensionality with the letter S (small) followed by the total number of blocks $\|B\|_1$. The full model is depicted in Figure 3.

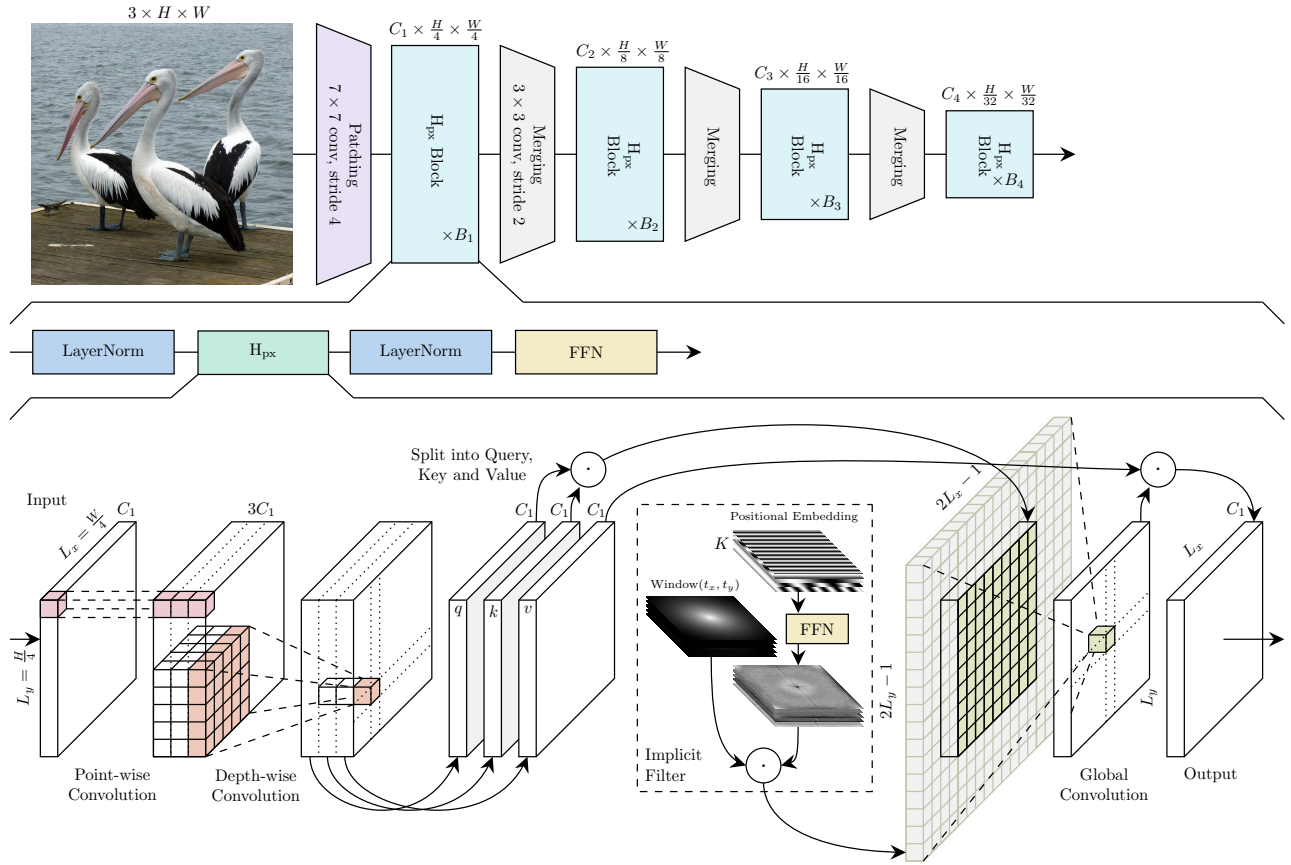


Figure 3: **The HyenaPixel (H_{px}) operator embedded in the MetaFormer framework.** The first row shows the MetaFormer framework [Yu *et al.*, 2024] with an input of size $H \times W$, typically set to 224 px^2 . The input is divided into 4×4 patches and processed by a sequence of H_{px} blocks with intermediate merging layers to reduce spatial resolution. The second row focuses on the structure of the H_{px} block with Layer Norm [Ba *et al.*, 2016] and a Feed Forward Network (FFN). The lower row shows the H_{px} operator. The input feature map has two spatial dimensions $L_y = \frac{H}{4}$ and $L_x = \frac{W}{4}$ and the channel dimension C_1 . First, the dimension is increased to $3C_1$ by a point-wise and a depth-wise 5×5 convolution. The resulting feature map is split into three equal-sized chunks: query q , key k , and value v . The result of the element-wise multiplication \odot of q and k is convolved with a global implicit filter. The final output is the element-wise multiplication with v .

Token mixer layout. The main layout has H_b or H_{px} in each stage of the network, that is H_b Former and H_{px} Former. The hyper-parameters of H_b are set to filter sizes $L = [2 \cdot 56^2 - 1, 2 \cdot 28^2 - 1, 2 \cdot 14^2 - 1, 2 \cdot 7^2 - 1]$, position embedding dimensions $K = [32, 32, 48, 64]$, and hidden filter projection dimensions of $2K_i$ for each stage i . H_{px} parameters are similar, with the difference that the kernel size is defined by $L_x = L_y = [111, 55, 27, 13]$. Global context, as provided by attention, proved beneficial in later stages [Yu *et al.*, 2024; Dong *et al.*, 2022]. Inspired by this observation, we also formulate the CH_{px} Former, with local convolutions in the first two and H_{px} in the last two stages. The local convolution follows the inverse separable convolution proposed in MobileNetV2 [Sandler *et al.*, 2018] that is also employed in the ConvFormer [Yu *et al.*, 2022] with a kernel size of 7. Furthermore, we propose H_{px} AFormer to evaluate whether attention has any additional value beyond the capabilities of H_{px} . H_{px} AFormer uses H_{px} in the first two stages, followed by the attention stages. Similarly, we define H_b AFormer.

4 Evaluation

4.1 Image Classification

Pre-training on ImageNet-1k. We train our models on ImageNet-1k [Deng *et al.*, 2009] (IN-1k) with 1000 classes. It consists of 1.3M and 50K images in the training and validation set, respectively. We follow the training strategy of Yu *et al.* [2024] and optimize with AdamW [Loshchilov and Hutter, 2019], a batch size of 4096, a learning rate of $4e^{-3}$, and weight decay of 0.05 for 310 epochs. The learning rate is scheduled with a linear warm-up for 20 epochs followed by cosine decay for 280 epochs with a final learning rate of $1e^{-5}$ and an additional 10 cool-down epochs. Regularization is added by Stochastic depth [Huang *et al.*, 2016] of 0.2, Label Smoothing [Szegedy *et al.*, 2016] with 0.1, and Res Scale [Shleifer *et al.*, 2021] in the last two stages.

We apply the following data augmentations: Mixup [Zhang *et al.*, 2018], Cutmix [Yun *et al.*, 2019], Rand-Augment [Cubuk *et al.*, 2020], and Random Erasing [Zhong *et al.*, 2020]. Our implementation is based on the *timm* framework [Wightman, 2019].

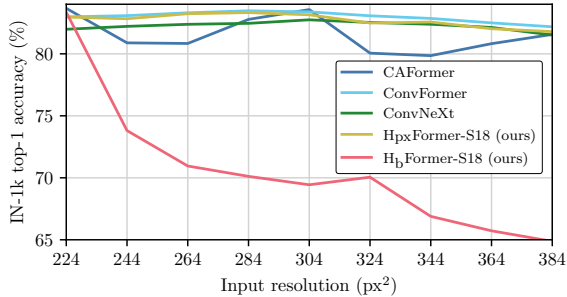


Figure 4: Robustness to resolution changes of different token mixer configurations. Token mixers with spatial and local bias scale well to higher resolutions without fine-tuning, while token mixers without bias fail or cause inconsistent results.

Fine-tuning on higher resolution. ConvNets naturally scale to different resolutions and show improved accuracy for higher resolution inputs [Tan and Le, 2019]. To test the effect of input resolution, we compute the accuracy for different resolutions for various models and visualize the results in Figure 4. Token mixers behave differently if the input resolution is increased. Networks with smaller filters (e.g. ConvFormer and ConvNeXt), are more robust against input resolution changes. CAFormer with convolution and attention layers shows instability, while the bias-free H_b Former shows a significant drop in accuracy. The behavior of H_b Former can be explained by the specialization on a specific input shape (cf. the visualization of filters in the supplementary material).

We fine-tune H_{px} Former-S18 on a higher resolution and follow a similar strategy applied to attention-based Transformers with positional embeddings [Dosovitskiy *et al.*, 2021] and re-sample the global filters. The resulting filters have a size of $L_x = L_y = [191, 95, 47, 23]$. We fine-tune the re-sampled model for an additional 30 epochs on IN-1k with a 384 px² resolution using AdamW, a learning rate of $5e-5$, a batch size of 1024, exponential moving average [Polyak and Juditsky, 1992] and head dropout of 0.4. Learning rate scheduling, Mixup and Cutmix are disabled.

Results on ImageNet-1k. Table 1 reports the results on IN-1k. For validation, typically a center-cropped region of the input image is selected with a crop size between 0.8 and 1.0 that maximizes the accuracy. However, this approach ignores the robustness against different object scales. To address this issue, we evaluate different models with crop sizes between 0.8 and 1.0 and a step size of 0.025. We utilize the `timm` package [Wightman, 2019] or the implementation provided by the authors to reevaluate the models. We report the mean and standard deviation next to the maximum accuracy and refer to the mean values as accuracy if not stated otherwise.

H_b Former-S18 beats ConvFormer-S18 by 0.5%, ConvNeXt-T by 1.33%, and Swin-T by 2.12% in accuracy and only builds on convolutional layers. The model is even comparable with some networks with double (Swin-S, ConvNeXt-S) or triple (RepLKNet-31B) the FLOP requirement. Large-convolution networks like SLaK-T are outperformed by 0.94% or achieve comparable performance such as RepLKNet-31B, while requiring significantly more

| Model | #param. | FLOP | Best | Mean \pm SD |
|-------------------------------------|---------|--------|------|------------------|
| 224 px² | | | | |
| Swin-T | 28M | 4.5G | 81.4 | 81.17 \pm 0.18 |
| ConvNeXt-T | 29M | 4.5G | 82.1 | 81.96 \pm 0.13 |
| SLaK-T | *30M | *5.0G | 82.5 | 82.35 \pm 0.14 |
| ConvFormer-S18 | 27M | 3.9G | 83.0 | 82.79 \pm 0.15 |
| CAFormer-S18 | 26M | 4.1G | 83.6 | 83.52 \pm 0.15 |
| CH_{px} Former-S18 (ours) | 28M | 4.3G | 83.0 | 82.82 \pm 0.15 |
| H_{px} Former-S18 (ours) | 29M | 4.8G | 83.0 | 82.87 \pm 0.14 |
| H_b Former-S18 (ours) | 27M | 4.4G | 83.2 | 83.14 \pm 0.16 |
| H_b Former-S18 (ours) | 28M | 4.4G | 83.5 | 83.29 \pm 0.15 |
| H_{px} AFormer-S18 (ours) | 28M | 4.6G | 83.6 | 83.41 \pm 0.19 |
| ConvNeXt-S | 50M | 8.7G | 83.2 | 83.03 \pm 0.16 |
| Swin-S | 50M | 8.7G | 83.3 | 83.11 \pm 0.18 |
| SLaK-S | *55M | *9.8G | 83.8 | - |
| ConvFormer-S36 | 40M | 7.6G | 84.0 | 83.89 \pm 0.17 |
| CAFormer-S36 | 39M | 8.0G | 84.5 | 84.38 \pm 0.15 |
| H_{px} / Conv (ours) | 56M | 8.7G | 83.8 | 83.58 \pm 0.15 |
| RepLKNet-31B | 79M | 15.3G | 83.5 | - |
| Swin-B | 88M | 15.4G | 83.6 | 83.43 \pm 0.17 |
| ConvNeXt-B | 89M | 15.4G | 83.9 | 83.78 \pm 0.15 |
| SLaK-B | *95M | *17.1G | 84.0 | - |
| ConvFormer-M36 | 57M | 12.8G | 84.5 | 84.29 \pm 0.16 |
| CAFormer-M36 | 56M | 13.2G | 85.1 | 84.98 \pm 0.14 |
| H_{px} / H_b / Conv / CA (ours) | 111M | 17.4G | 84.5 | 84.37 \pm 0.15 |
| 384 px² | | | | |
| ConvFormer-S18 | 27M | 11.6G | 84.4 | 84.11 \pm 0.28 |
| H_{px} Former-S18 (ours) | 33M | 14.1G | 84.2 | 83.99 \pm 0.23 |

Table 1: **IN-1k validation set results.** We compare our results with the Swin Transformer [Liu *et al.*, 2021], ConvNeXt [Liu *et al.*, 2022], Conv- and CAFormer [Yu *et al.*, 2024], RepLKNet [Ding *et al.*, 2022] and SLaK [Liu *et al.*, 2023]. We report the parameter counts, estimated FLOP using `fvcore` [Contributors, 2019], the best and the mean top-1 accuracy with standard deviation (SD) over a range of crop proportions between 0.8 and 1.0. Note that the parameter and FLOP counts of SLaK models marked with a * require specialized hardware supporting sparse convolution.

parameters and FLOPs.

Bidirectional modeling and the Hyena formulation seem to be more valuable than locality and spatial bias. By adding spatial bias to Hyena in the form of H_{px} Former-S18, the advantage is reduced to 0.08%. The advantage shrinks to 0.03% if local convolutions are utilized in the first two stages, i.e. CH_{px} Former.

In comparison to CAFormer-S18 with additional attention layers, H_b Former-S18 is 0.23% behind. Combining attention with H_b further increases the difference to -0.38% while attention and H_{px} reduce the gap to -0.11% . Differences in optimizer choice, the preference of local features in earlier stages (see Section 5), the incompatibility of learned features, and the higher robustness against resolution changes of convolution (cf. Figure 4) could be responsible.

We find that H_{px} Former-S18 and ConvFormer-S18 differ in about 50% of the wrongly classified images, indicating a different solution. The best accuracy improves to 83.8% with

| | Best acc. | Mean \pm SD |
|---------------------------------------|-----------|------------------|
| H _{px} Former-S12 (Baseline) | 80.3 | 80.15 \pm 0.19 |
| Kernel Size for Global Convolution | | |
| $[55^2, 27^2, 13^2, 7^2]$ | 80.3 | 80.14 \pm 0.16 |
| $[27^2, 13^2, 7^2, 3^2]$ | 80.1 | 79.97 \pm 0.17 |
| $[9^2, 9^2, 9^2, 9^2]$ | 80.3 | 80.13 \pm 0.12 |
| Token Mixer | | |
| Hyena | 79.9 | 79.77 \pm 0.11 |
| H _b | 81.0 | 80.79 \pm 0.13 |
| H _{px} with Separable Conv. | 79.9 | 79.75 \pm 0.13 |
| Pooling Layer | | |
| Attention Pooling with Registers | 80.2 | 79.99 \pm 0.16 |
| Network Depth | | |
| H _{px} Former-S4 | 73.4 | 73.24 \pm 0.11 |
| ConvFormer-S4 | 73.0 | 72.83 \pm 0.09 |

Table 2: Effect of different H_{px}Former-S12 ablations on the IN-1k top-1 accuracy. Best and mean accuracy \pm SD as in Tab. 1.

a simple ensemble of these two models by mean pooling the predictions. By adding H_bFormer-S18 and CAFormer-S18 to the ensemble the best accuracy further increases to 84.5%.

The lower part of Tab. 1 reports results for higher-resolution images. Fine-tuning on a resolution of 384px² puts ConvFormer-S18 ahead of H_{px}Former-S18 by 0.12%.

First of all, our results support the assumptions on the MetaFormer as baseline model and the expressiveness of Hyena. Interestingly, we observe that features produced by different token mixers can be incompatible. Moreover, we close the gap between ConvNets and Transformers by a radical new approach: A ConvNet for vision without spatial bias.

4.2 Ablation Study

We test different aspects of H_{px}Former-S12. The training is conducted on IN-1k and mainly follows the procedure described in Section 4.1, but we reduce the number of epochs from 310 to 160 and adjust the cosine decay accordingly. Table 2 reports the results of the ablation study.

Kernel size. The global convolution is the main component of H_{px} and is almost twice as large as the feature map, such that each output position can “see” all input positions, similar to attention. Reducing the kernel size marginally decreases mean accuracy. Once later stages lose global context, we observe an accuracy drop of 0.16% while missing global context in earlier stages has almost no negative impact.

Other token mixers. We already compared the runtime of different token mixers (see Figure 2). The capabilities of different token mixers can also vary drastically even in the same architecture [Yu *et al.*, 2024], though. Bidirectional instead of causal sequence modeling with Hyena (H_b) significantly boosts the mean accuracy (+1.02%). Adding spatial bias (H_{px}) decreases the performance by 0.64%. We observed that H_{px} prefers sub-optimal solutions focusing on the horizontal and vertical direction while H_b shows more complex kernels (see the kernel visualizations in the supplementary material). Furthermore, the image border is more prominent in H_{px}, due

| Model | AP ^{box} | AP ₅₀ ^{box} | AP ₇₅ ^{box} | AP ^{mask} | AP ₅₀ ^{mask} | AP ₇₅ ^{mask} |
|-----------------------------------|-------------------|---------------------------------|---------------------------------|--------------------|----------------------------------|----------------------------------|
| Swin-T | 50.4 | 69.2 | 54.7 | 43.7 | 66.6 | 47.3 |
| ConvNeXt-T | 50.4 | 69.1 | 54.8 | 43.7 | 66.5 | 47.3 |
| SLaK-T | 51.3 | 70.0 | 55.7 | 44.3 | 67.2 | 48.1 |
| ConvFormer-S18 | 51.5 | 70.7 | 55.8 | 44.6 | 67.8 | 48.2 |
| CAFormer-S18 | 52.3 | 71.3 | 56.9 | 45.2 | 68.6 | 48.8 |
| H _{px} Former-S18 (ours) | 51.5 | 70.0 | 56.0 | 44.6 | 67.6 | 48.2 |

Table 3: Object detection and instance segmentation results on the MS COCO validation set with Cascade Mask R-CNN.

to 3 \times more zero values in the input. To test our hypothesis, we replace the Hyena convolution with spatially separable convolutions focusing on the main axes and observe a further drop in accuracy by -0.4% . We hypothesize that more complex positional embeddings could improve H_{px}, however, this remains for future work.

Attention pooling with register tokens. Attention pooling selects relevant tokens within a sequence based on learned queries [Touvron *et al.*, 2021b]. Intuitively, this helps the network to focus on certain parts of the feature map, like foreground pixels. We extend attention pooling by register tokens [Darcet *et al.*, 2023] to act as an “attention fallback” if the image contents are irrelevant to the query token. Mean pooling outperforms attention pooling by 0.16%.

Network depth and context size. While ConvNets typically require many layers to view the complete input image, H_{px} ideally only requires one layer. We investigate whether we can reduce network depth while increasing a layer’s context size, by creating two shallow networks: H_{px}Former-S4 and ConvFormer-S4 with one block per stage. The accuracy on IN-1k differs by 0.41% in favor of H_{px}Former. This supports our hypothesis, however, building a large ERF with a hierarchical structure and small kernels is also effective, because of its multiplicative effect on the receptive field [Luo *et al.*, 2016].

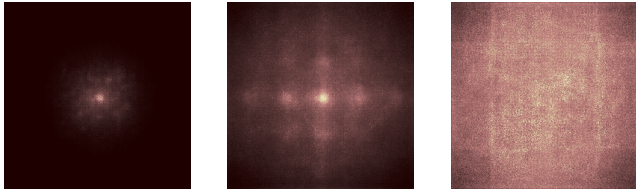
4.3 Downstream Tasks

Object Detection and Instance Segmentation on MS COCO. In the same way as ConvNeXt [Liu *et al.*, 2022], we evaluate the localization properties of H_{px} with Cascade Mask R-CNN [Cai and Vasconcelos, 2018] on MSCOCO [Lin *et al.*, 2014]. With the MMDetection framework [Chen *et al.*, 2019], we train the model with AdamW, a batch size of 16, and a learning rate of $2e^5$ for a 3 \times schedule (36 epochs), halving the learning rate after 27 and 33 epochs. Table 3 reports the results. H_{px}Former-S18 shows a drop in AP^{box} of -0.8 and AP^{mask} of -0.6 , compared to CAFormer-S18. H_{px}Former-S18 performs on par with ConvFormer-S18 with significantly smaller kernels.

Semantic Segmentation on ADE20k. We evaluate the downstream performance on semantic segmentation with UperNet [Xiao *et al.*, 2018] on the ADE20k benchmark [Zhou *et al.*, 2019], following ConvNeXt [Liu *et al.*, 2022]. We base our implementation on MMSegmentation [Contributors, 2020] and train for 160k steps. Table 4 reports the results. H_{px}Former-S18 beats Swin-T by 1.6 mIoU

| Model | mIoU |
|----------------------------|-------|
| Swin-T | 44.5 |
| ConvNeXt-T | 46.0 |
| SLaK-T | 47.6 |
| ConvFormer-S18 | *48.6 |
| CAFormer-S18 | *48.9 |
| H_{px} Former-S18 (ours) | 46.1 |

Table 4: Semantic segmentation on ADE20k validation set with an input resolution of 512^2 . Models marked * use multi-scale testing.



(a) ConvFormer-S18 (b) SLaK-T (c) H_{px} Former-S18

Figure 5: Effective Receptive Field (ERF) of different models sampled over 50 images of size $1024px^2$ from the IN-1k validation set.

and ConvNeXt by 0.1 mIoU, while staying 1.5 mIoU behind SLaK-T. This is in contrast to the observation by Liu et al. [2023] that larger kernels improve results.

5 Analysis

Effective receptive field. The Effective Receptive Field (ERF) measures the influence of each input pixel on the center-most output value by tracking the gradients in a backward pass [Luo et al., 2016]. A large ERF is often associated with a better performance in vision tasks [Ding et al., 2022; Liu et al., 2023]. We follow related work [Ding et al., 2022; Liu et al., 2023] and compare the ERF [Kim et al., 2023]. Figure 5 shows the ERFs of three models. ConvFormer and SLaK have a strong local bias caused by local convolutions as main building blocks. SLaK features off-center areas with high gradients caused by the separable sparse convolution. H_{px} Former has a large ERF with no obvious center location, but some vertical and horizontal artifacts. Further ERF visualizations are provided in the supplementary material.

We hypothesize that H_{px} could benefit from an additional residual connection with a small convolution. This could be particularly helpful for localization tasks. We leave this study for future research.

Truncate kernel in trained models. Due to the learnable decay parameter in H_{px} , we can estimate the required kernel size at different depths. By setting all values of $\text{Window}(t_x, t_y)$ to zero that are smaller than 0.05, we can measure the diameter of the non-zero values. Figure 6 shows the mean relative feature map coverage of the global convolution in each block. One can observe that H_{px} learns the same kernel sizes at the same stage regardless of other token mixers involved in earlier or later stages. The coverage in each stage stays almost constant while former layers of a stage have slightly larger kernels. We truncate the filters

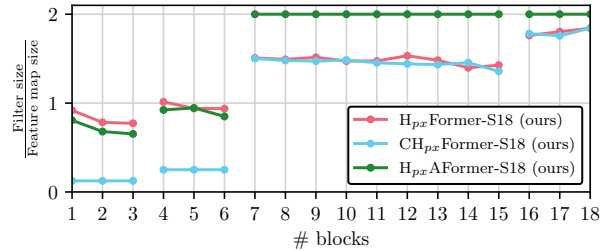


Figure 6: Learned filter sizes in H_{px} Former-S18 relative to feature map sizes at different network depths. For attention, we set the relative feature map coverage to 2 and for convolution we use the actual kernel size. Note that the feature map coverage can be larger than 1 because the kernel size of H_{px} is almost twice the feature map size.

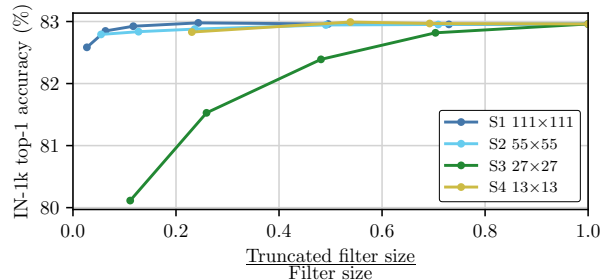


Figure 7: Impact of truncated filters in H_{px} Former-S18 on the top-1 IN-1k accuracy. For each stage (S), we modify the large kernels within the current stage by setting all values to zero that are larger than the relative filter size.

within each stage of a pre-trained H_{px} Former-S18 and visualize the IN-1k classification results in Figure 7. The truncation of Stage 3 has the biggest impact with an accuracy drop of almost 2.9%. Surprisingly, the first and last stage is more local and can even benefit from truncation, improving performance slightly by 0.04%. These insights might help constructing better model layouts.

6 Conclusion

In this work, we studied whether the Hyena operator is a sufficient replacement for the attention token mixer in computer vision applications. To this end, we extended Hyena to non-causal, bidirectional sequence modeling and added 2D spatial bias. We found the Hyena formulation useful for training extremely large kernels up to 191×191 . Analyzing trained models with these token mixers showed that bidirectional modeling is sufficient to achieve competitive performance, while spatial bias hurts the final performance. Large kernel sizes do not improve performance for downstream tasks that require localization, though. Our analysis showed that the ERF for our two-dimensional Hyena lacks the local bias present in other approaches.

In conclusion, our results clearly suggest large, non-causal bidirectional, spatially unbiased convolution as a promising avenue for future research.

Acknowledgments

This research has been funded by the Federal Ministry of Education and Research of Germany under grant no. 01IS22094E WEST-AI.

References

- [Ba *et al.*, 2016] L. J. Ba, J. R. Kiros, and G. E. Hinton. Layer normalization. *CoRR*, abs/1607.06450, 2016.
- [Behnke, 2003] S. Behnke. *Hierarchical Neural Networks for Image Interpretation*, volume 2766 of *Lecture Notes in Computer Science*. Springer, 2003.
- [Cai and Vasconcelos, 2018] Z. Cai and N. Vasconcelos. Cascade R-CNN: Delving into high quality object detection. In *CVPR*, pages 6154–6162, 2018.
- [Chen *et al.*, 2019] K. Chen, J. Wang, J. Pang, Y. Cao, Y. Xiong, et al. MMDetection: Open MMLab detection toolbox and benchmark. *CoRR*, abs/1906.07155, 2019.
- [Ciresan *et al.*, 2012] D. C. Ciresan, U. Meier, and J. Schmidhuber. Multi-column deep neural networks for image classification. In *CVPR*, pages 3642–3649, 2012.
- [Contributors, 2019] Contributors. fvcore Library. <https://github.com/facebookresearch/fvcore>, 2019.
- [Contributors, 2020] Contributors. MMSegmentation: OpenMMLab semantic segmentation toolbox and benchmark. <https://github.com/open-mmlab/mms Segmentation>, 2020.
- [Cubuk *et al.*, 2020] E. D. Cubuk, B. Zoph, J. Shlens, and Q. V. Le. Randaugment: Practical automated data augmentation with a reduced search space. In *CVPR*, pages 3008–3017, 2020.
- [Dai *et al.*, 2017] J. Dai, H. Qi, Y. Xiong, Y. Li, G. Zhang, H. Hu, and Y. Wei. Deformable convolutional networks. In *ICCV*, pages 764–773, 2017.
- [Darcet *et al.*, 2023] T. Darcet, M. Oquab, J. Mairal, and P. Bojanowski. Vision transformers need registers. *CoRR*, abs/2309.16588, 2023.
- [Deng *et al.*, 2009] J. Deng, W. Dong, R. Socher, L. Li, K. Li, and L. Fei-Fei. ImageNet: A large-scale hierarchical image database. In *CVPR*, pages 248–255, 2009.
- [Ding *et al.*, 2022] X. Ding, X. Zhang, J. Han, and G. Ding. Scaling up your kernels to 31x31: Revisiting large kernel design in cnns. In *CVPR*, pages 11963–11975, 2022.
- [Dong *et al.*, 2022] X. Dong, J. Bao, D. Chen, W. Zhang, N. Yu, L. Yuan, D. Chen, and B. Guo. CSWin Transformer: A general vision transformer backbone with cross-shaped windows. In *CVPR*, pages 12114–12124, 2022.
- [Dosovitskiy *et al.*, 2021] A. Dosovitskiy, L. Beyer, A. Kolesnikov, D. Weissenborn, X. Zhai, T. Unterthiner, M. Dehghani, M. Minderer, G. Heigold, S. Gelly, J. Uszkoreit, and N. Houlsby. An image is worth 16x16 words: Transformers for image recognition at scale. In *ICLR*, 2021.
- [Fu *et al.*, 2023] D. Y. Fu, E. L. Epstein, E. Nguyen, A. W. Thomas, M. Zhang, T. Dao, A. Rudra, and C. Ré. Simple hardware-efficient long convolutions for sequence modeling. In *ICML*, pages 10373–10391, 2023.
- [Guo *et al.*, 2022] M. Guo, C. Lu, Q. Hou, Z. Liu, M. Cheng, and S. Hu. SegNeXt: Rethinking convolutional attention design for semantic segmentation. In *NeurIPS*, 2022.
- [Han *et al.*, 2023] D. Han, X. Pan, Y. Han, S. Song, and G. Huang. Flatten Transformer: Vision transformer using focused linear attention. In *ICCV*, pages 5961–5971, 2023.
- [He *et al.*, 2016] K. He, X. Zhang, S. Ren, and J. Sun. Deep residual learning for image recognition. In *CVPR*, pages 770–778, 2016.
- [Hendrycks and Gimpel, 2016] D. Hendrycks and K. Gimpel. Gaussian error linear units (GELUs). *CoRR*, abs/1606.08415, 2016.
- [Huang *et al.*, 2016] G. Huang, Y. Sun, Z. Liu, D. Sedra, and K. Q. Weinberger. Deep networks with stochastic depth. In *ECCV*, pages 646–661, 2016.
- [Katharopoulos *et al.*, 2020] A. Katharopoulos, A. Vyas, N. Pappas, and F. Fleuret. Transformers are RNNs: Fast autoregressive transformers with linear attention. In *ICML*, pages 5156–5165, 2020.
- [Kim *et al.*, 2023] B. J. Kim, H. Choi, H. Jang, D. G. Lee, W. Jeong, and S. W. Kim. Dead pixel test using effective receptive field. *Pattern Recognition Letters*, 167:149–156, 2023.
- [Krizhevsky *et al.*, 2012] A. Krizhevsky, I. Sutskever, and G. E. Hinton. ImageNet classification with deep convolutional neural networks. In *NeurIPS*, pages 1106–1114, 2012.
- [LeCun *et al.*, 1989] Y. LeCun, B. Boser, J. S. Denker, D. Henderson, R. E. Howard, W. Hubbard, and L. D. Jackel. Backpropagation applied to handwritten zip code recognition. *Neural Computation*, 1(4):541–551, 1989.
- [LeCun *et al.*, 1998] Y. LeCun, L. Bottou, Y. Bengio, and P. Haffner. Gradient-based learning applied to document recognition. *Proc. IEEE*, pages 2278–2324, 1998.
- [Lee-Thorp *et al.*, 2022] J. Lee-Thorp, J. Ainslie, I. Eckstein, and S. Ontañón. FNet: Mixing tokens with Fourier transforms. In *NAACL-HLT*, pages 4296–4313, 2022.
- [Lin *et al.*, 2014] T. Lin, M. Maire, S. J. Belongie, J. Hays, P. Perona, D. Ramanan, P. Dollár, and C. L. Zitnick. Microsoft COCO: common objects in context. In *ECCV*, pages 740–755, 2014.
- [Liu *et al.*, 2021] Z. Liu, Y. Lin, Y. Cao, H. Hu, Y. Wei, Z. Zhang, S. Lin, and B. Guo. Swin Transformer: Hierarchical vision transformer using shifted windows. In *ICCV*, pages 9992–10002, 2021.
- [Liu *et al.*, 2022] Z. Liu, H. Mao, C. Wu, C. Feichtenhofer, T. Darrell, and S. Xie. A ConvNet for the 2020s. In *CVPR*, pages 11966–11976, 2022.

- [Liu *et al.*, 2023] S. Liu, T. Chen, X. Chen, X. Chen, Q. Xiao, B. Wu, T. Kärkkäinen, et al. More ConvNets in the 2020s: Scaling up kernels beyond 51x51 using sparsity. In *ICLR*, 2023.
- [Loshchilov and Hutter, 2019] I. Loshchilov and F. Hutter. Decoupled weight decay regularization. In *ICLR*, 2019.
- [Luo *et al.*, 2016] W. Luo, Y. Li, R. Urtasun, and R. S. Zemel. Understanding the effective receptive field in deep convolutional neural networks. In *NeurIPS*, pages 4898–4906, 2016.
- [Peng *et al.*, 2017] C. Peng, X. Zhang, G. Yu, G. Luo, and J. Sun. Large kernel matters - improve semantic segmentation by global convolutional network. In *CVPR*, pages 1743–1751, 2017.
- [Poli *et al.*, 2023] M. Poli, S. Massaroli, E. Nguyen, D. Y. Fu, T. Dao, S. A. Baccus, Y. Bengio, S. Ermon, and C. Ré. Hyena Hierarchy: Towards larger convolutional language models. In *ICML*, pages 28043–28078, 2023.
- [Polyak and Juditsky, 1992] B. T. Polyak and A. B. Juditsky. Acceleration of stochastic approximation by averaging. *SIAM Journal on Control and Optimization*, 30(4):838–855, 1992.
- [Romero *et al.*, 2022a] D. W. Romero, R. Bruintjes, J. M. Tomczak, E. J. Bekkers, M. Hoogendoorn, and J. van Gemert. FlexConv: Continuous kernel convolutions with differentiable kernel sizes. In *ICLR*, 2022.
- [Romero *et al.*, 2022b] D. W. Romero, A. Kuzina, E. J. Bekkers, J. M. Tomczak, and M. Hoogendoorn. CK-Conv: Continuous kernel convolution for sequential data. In *ICLR*, 2022.
- [Sandler *et al.*, 2018] M. Sandler, A. G. Howard, M. Zhu, A. Zhmoginov, and L. Chen. MobileNetV2: Inverted residuals and linear bottlenecks. In *CVPR*, pages 4510–4520, 2018.
- [Shleifer *et al.*, 2021] S. Shleifer, J. Weston, and M. Ott. NormFormer: Improved transformer pretraining with extra normalization. *CoRR*, abs/2110.09456, 2021.
- [Simonyan and Zisserman, 2015] Karen Simonyan and Andrew Zisserman. Very deep convolutional networks for large-scale image recognition. In *ICLR*, 2015.
- [Smith *et al.*, 2023] S. L. Smith, A. Brock, L. Berrada, and S. De. ConvNets match vision transformers at scale. *CoRR*, abs/2310.16764, 2023.
- [Szegedy *et al.*, 2015] C. Szegedy, W. Liu, Y. Jia, P. Sermanet, S. E. Reed, D. Anguelov, D. Erhan, V. Vanhoucke, and A. Rabinovich. Going deeper with convolutions. In *CVPR*, pages 1–9, 2015.
- [Szegedy *et al.*, 2016] C. Szegedy, V. Vanhoucke, S. Ioffe, J. Shlens, and Z. Wojna. Rethinking the Inception architecture for computer vision. In *CVPR*, pages 2818–2826, 2016.
- [Tan and Le, 2019] M. Tan and Q. V. Le. EfficientNet: Rethinking model scaling for convolutional neural networks. In *ICML*, pages 6105–6114, 2019.
- [Tolstikhin *et al.*, 2021] I. O. Tolstikhin, N. Houlsby, A. Kolesnikov, L. Beyer, X. Zhai, T. Unterthiner, J. Yung, A. Steiner, D. Keysers, J. Uszkoreit, M. Lucic, and A. Dosovitskiy. MLP-Mixer: An all-MLP architecture for vision. In *NeurIPS*, pages 24261–24272, 2021.
- [Touvron *et al.*, 2021a] H. Touvron, M. Cord, M. Douze, F. Massa, A. Sablayrolles, and H. Jégou. Training data-efficient image transformers & distillation through attention. In *ICML*, pages 10347–10357, 2021.
- [Touvron *et al.*, 2021b] H. Touvron, M. Cord, A. El-Nouby, P. Bojanowski, A. Joulin, G. Synnaeve, and H. Jégou. Augmenting convolutional networks with attention-based aggregation. *CoRR*, abs/2112.13692, 2021.
- [Tu *et al.*, 2022] Z. Tu, H. Talebi, H. Zhang, F. Yang, P. Milanfar, A. C. Bovik, and Y. Li. MaxViT: Multi-axis vision transformer. In *ECCV*, pages 459–479, 2022.
- [Vaswani *et al.*, 2017] A. Vaswani, N. Shazeer, N. Parmar, J. Uszkoreit, L. Jones, A. N. Gomez, L. Kaiser, and I. Polosukhin. Attention is all you need. In *NeurIPS*, pages 5998–6008, 2017.
- [Wagner *et al.*, 2019] J. Wagner, J. M. Köhler, T. Gindele, L. Hetzel, J. T. Wiedemer, and S. Behnke. Interpretable and fine-grained visual explanations for convolutional neural networks. In *CVPR*, pages 9097–9107, 2019.
- [Wang and Liu, 2021] Z. Wang and J. Liu. Translating math formula images to LaTeX sequences using deep neural networks with sequence-level training. *Int. J. Document Anal. Recognit.*, 24(1):63–75, 2021.
- [Wightman, 2019] R. Wightman. PyTorch image models. <https://github.com/rwightman/pytorch-image-models>, 2019.
- [Woo *et al.*, 2023] S. Woo, S. Debnath, R. Hu, X. Chen, Z. Liu, I. S. Kweon, and S. Xie. ConvNeXt V2: Co-designing and scaling ConvNets with masked autoencoders. In *CVPR*, pages 16133–16142, 2023.
- [Xiao *et al.*, 2018] T. Xiao, Y. Liu, B. Zhou, Y. Jiang, and J. Sun. Unified perceptual parsing for scene understanding. In *ECCV*, pages 432–448, 2018.
- [Yu *et al.*, 2022] W. Yu, M. Luo, P. Zhou, C. Si, Y. Zhou, X. Wang, J. Feng, and S. Yan. MetaFormer is actually what you need for vision. In *CVPR*, pages 10809–10819, 2022.
- [Yu *et al.*, 2024] W. Yu, C. Si, P. Zhou, M. Luo, Y. Zhou, J. Feng, S. Yan, and X. Wang. MetaFormer baselines for vision. *IEEE TPAMI*, 46(2):896–912, 2024.
- [Yun *et al.*, 2019] S. Yun, D. Han, S. Chun, S. J. Oh, Y. Yoo, and J. Choe. CutMix: Regularization strategy to train strong classifiers with localizable features. In *ICCV*, pages 6022–6031, 2019.
- [Zhang *et al.*, 2018] H. Zhang, M. Cissé, Y. N. Dauphin, and D. Lopez-Paz. mixup: Beyond empirical risk minimization. In *ICLR*, 2018.
- [Zhong *et al.*, 2020] Z. Zhong, L. Zheng, G. Kang, S. Li, and Y. Yang. Random erasing data augmentation. In *AAAI*, pages 13001–13008, 2020.

- [Zhou *et al.*, 2019] B. Zhou, H. Zhao, X. Puig, T. Xiao, S. Fidler, A. Barriuso, and A. Torralba. Semantic understanding of scenes through the ADE20K dataset. *IJCV*, 127(3):302–321, 2019.
- [Zimmerman and Wolf, 2023] I. Zimmerman and L. Wolf. Multi-dimensional hyena for spatial inductive bias. *CoRR*, abs/2309.13600, 2023.

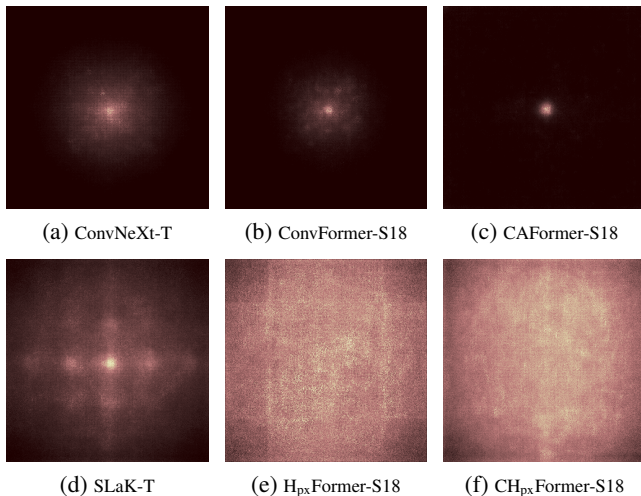


Figure 8: Effective Receptive Field (ERF) of different models sampled over 50 images of size 1024px^2 drawn from the IN-1k validation set.

A Overview

In this supplementary material to the paper “HyenaPixel: Global Image Context with Convolutions”, we investigate the properties and learned weights of our non-causal Hyena (H_b) and HyenaPixel (H_{px}) operators. We extend our investigation of the Effective Receptive Field (ERF) in Sec. B for different models. Furthermore, we provide visual explanations for models with small and large filters to study the important pixels for categorization (Sec. C). Finally, we look at the learned kernels of H_b and H_{px} with the goal to gain insight into the effect of large filter sizes and spatial bias on the filter structure (Sec. D).

B Effective Receptive Field

The Effective Receptive Field (ERF) measures the influence of each input pixel on the centermost output value by tracking the gradients in a backward pass [Luo *et al.*, 2016]. A large ERF is often associated with a better performance in vision tasks [Ding *et al.*, 2022; Liu *et al.*, 2023]. We follow related work [Ding *et al.*, 2022; Liu *et al.*, 2023] and compare the ERF [Kim *et al.*, 2023] by sampling 50 images from the ImageNet-1k (IN-1k) validation set with a resolution of 1024px^2 .

Fig. 8 compares the ERFs of six models. ConvNeXt [Liu *et al.*, 2022] and ConvFormer [Yu *et al.*, 2024] share similar bell-shaped fields with a local bias, with the ERF of ConvNeXt being slightly larger. Applying attention [Vaswani *et al.*, 2017] layers in the last two stages (i.e., CAFormer [Yu *et al.*, 2024]) increases the local focus. However, the model also interacts with more distant image regions to a smaller extent. Next to local bias, SLaK [Liu *et al.*, 2023] features off-center areas with high gradients caused by the separable sparse convolution. In contrast, H_{px} Former has no areas of high gradient or center location. Instead, the ERF covers the entire input image with a slight drop-off at the edges. Small convolutions in the first two stages (i.e., CH_{px} Former) still do

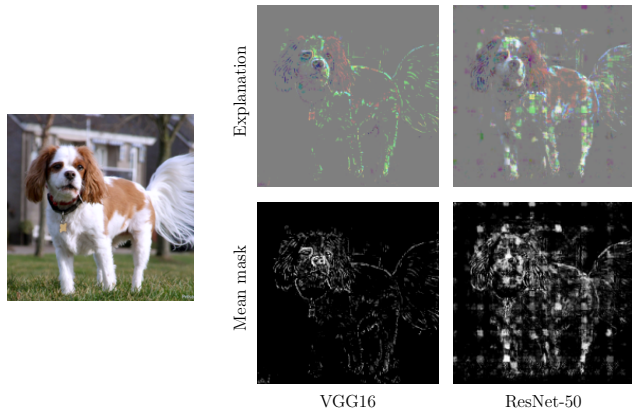


Figure 9: Fine-grained visual explanations (right) of an input image (left) generated with the FGVis method [Wagner *et al.*, 2019]. The explanation is calculated by multiplying the image x with the inverse mask $1 - m$. We add a gray scale image multiplied by m for better visibility. The mean mask is the mean value along the color channel of m . The mask values are raised by exponentiation with 7 for better visibility. The input image is from the IN-1k validation set.

not add local bias but smooth the ERF.

C Fine-grained Visual Explanations

Visual explanations can be formulated as an optimization problem: Find a mask that selects all pixels relevant to the object class with the highest probability. When this mask is subtracted from the original image, the highest class probability will switch on a different category. One issue with this approach is that it can also produce or favor adversarial masks. We utilize the adversarial defense and visualization method FGVis proposed by Wagner *et al.* [2019] by masking gradients that would move the output of activation layers beyond an upper or lower bound. The bounds are determined by measuring the outputs of these layers with the unmasked image of interest. We follow the training strategy proposed by [Wagner *et al.*, 2019]. The loss function is given by

$$y_e - \lambda \|m\|_1, \quad (5)$$

where y_e is the softmax score of the target class for the evidence $e = x \cdot m$ of the input image x and the mask m . λ is the weight of the sparsity term. We optimize for 500 iterations with SGD and a learning rate of 0.1. The weight mask is initialized to 1. The training is stopped early if the class with highest softmax score changes. The value of λ is determined by decreasing its value, starting at $\lambda = 1e^{-4}$, until the first early stopping criterion is met. We add further regularization by normalizing the gradient, clamping the mask values between 0 and 1, and adding noise to the input.

Fig. 9 shows explanations for VGG [Simonyan and Zisserman, 2015] and ResNet [He *et al.*, 2016]. VGG has a clear focus on the dog’s head and edge information. ResNet also incorporates texture information and other body parts for categorization. In addition, we also find the checkerboard pattern. This pattern is attributed to architectural details [Wagner *et al.*, 2019].

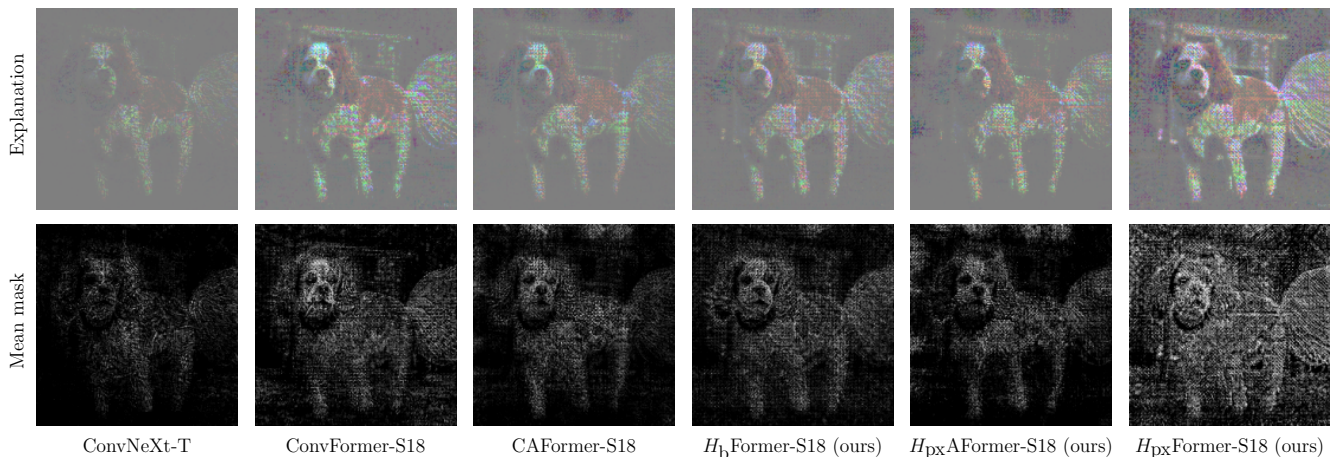


Figure 10: Fine-grained visual explanations for different models generated with the FGVis method [Wagner *et al.*, 2019]. Fig. 9 shows and explains the input image and the visualization strategy.

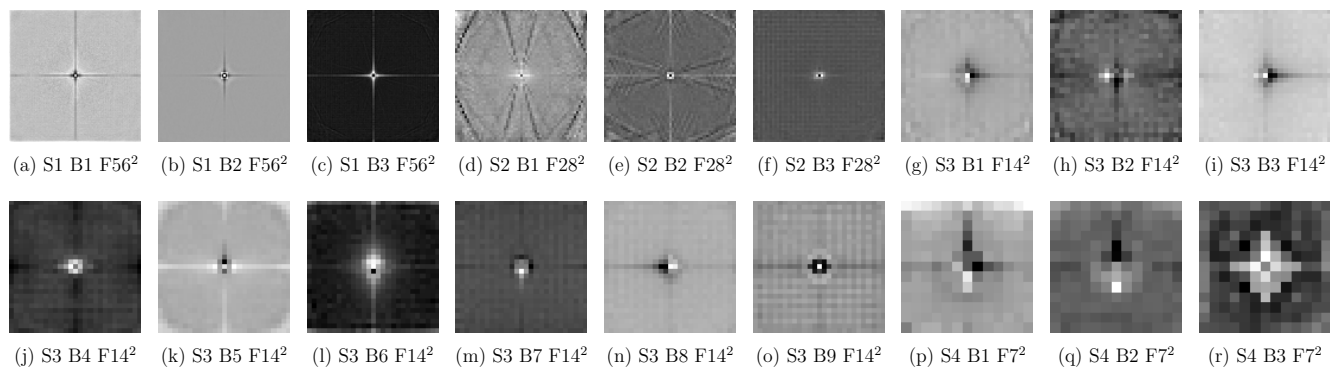


Figure 11: Normalized mean kernel weights for the 2D global convolution layers in the H_{px} Former-S18 by stage (S), block (B) and feature map size F . The width and height of the kernel is given by $2F - 1$, which provides the kernel with almost four times as many elements as the feature map.

Fig. 10 shows explanations for Transformer-based [Vaswani *et al.*, 2017] architectures. The resulting explanations are smoother and more dense than those produced by classical convolutional neural networks (ConvNets), c.f. Fig. 9. For all models there is some influence by the background, while ConvNeXt has the lowest and H_{px} Former has the highest background dependency. The models focus on texture and the dog’s facial features. H_{px} Former and ConvFormer are also dependent on edge information. This dependency disappears when the last two stages are filled with attention layers instead (CAFormer and H_{px} AFormer) and even adds an offset to the inside relative to the border. Interestingly, networks with attention also focus on regions with low information density, such as the house’s roof. This phenomenon is most likely related to register tokens [Darcet *et al.*, 2023].

D Learned Convolution Kernels

We visualize the learned global convolution kernels of H_{px} Former-S18 with spatial bias and H_b without spatial bias. Fig. 11 shows the kernels of H_{px} . The horizontal and ver-

tical lines are the most prominent features. Earlier stages show a clear center focus, while later stages can have high magnitude off-center elements. Furthermore, some filters feature grid patterns or even patterns that could be described as snowflake shaped. Similar structures can be observed in the filters learned by H_b Former depicted in Fig. 12. However, H_b filters appear smoother and better centered. We hypothesize that the sequential modeling increases the robustness against edge effects. Also, this naturally increases the complexity of the filter, as the 1D filters wrap around the image edges, effectively creating a unique filter for each position.

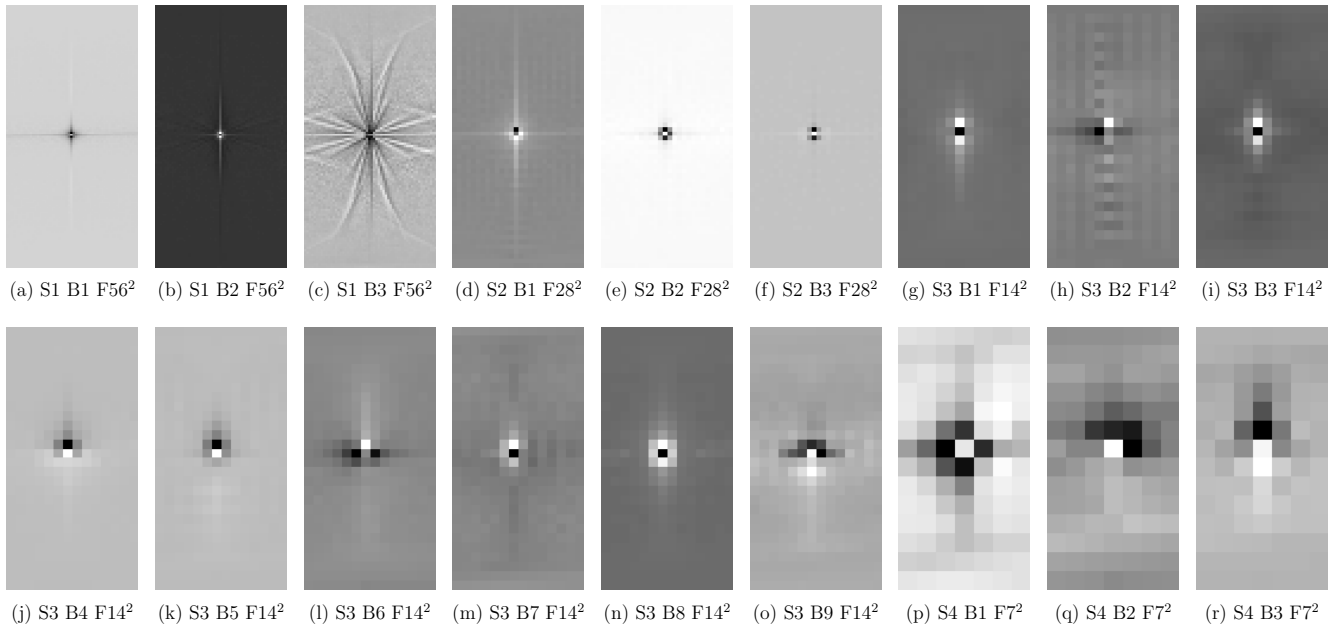


Figure 12: Normalized and reshaped mean kernel weights for the 1D global convolution layers in the H_bFormer-S18 by stage (S), block (B) and feature map size F . The kernel size is defined by $2F^2 - 1$. The visualization is not square because the 1D filter has $F^2 - 1$ more elements than the feature map, and we reshape the filter with a fixed width of F to account for the wrapping. Note that the visualization only shows the 2D reconstruction for the centermost pixel. The kernel would wrap differently at other evaluation positions due to the nature of the 1D convolution and the flattened input image.